Extracellular Protons Inhibit Charge Immobilization in the Cardiac Voltage-Gated Sodium Channel

D. K. Jones, T. W. Claydon, and P. C. Ruben*
Department of Biomedical Physiology and Kinesiology, Simon Fraser University, Burnaby, British Columbia, Canada

ABSTRACT Low pH depolarizes the voltage-dependence of cardiac voltage-gated sodium ($Na_V1.5$) channel activation and fast inactivation and destabilizes the fast-inactivated state. The molecular basis for these changes in protein behavior has not been reported. We hypothesized that changes in the kinetics of voltage sensor movement may destabilize the fast-inactivated state in $Na_V1.5$. To test this idea, we recorded $Na_V1.5$ gating currents in *Xenopus* oocytes using a cut-open voltage-clamp with extracellular solution titrated to either pH 7.4 or pH 6.0. Reducing extracellular pH significantly depolarized the voltage-dependence of both the Q_{ON}/V and Q_{OFF}/V curves, and reduced the total charge immobilized during depolarization. We conclude that destabilized fast-inactivation and reduced charge immobilization in $Na_V1.5$ at low pH are functionally related effects.

INTRODUCTION

Voltage-gated sodium (Na_V) channels are responsible for action potential generation and propagation in most excitable cells. Each channel is composed of a pore-forming α-subunit and one or more modulating β-subunits (1–4). The α-subunit forms the functional pore of the channel and is composed of four homologous domains (DI–DIV), each consisting of six transmembrane helical segments (S1–S6) (1,5). Helices S5 and S6, and the extracellular loops linking them (P-loops), combine to form the channel pore and selectivity filter (6). The S1–S4 helices form the voltage-sensing domain (VSD). Voltage sensitivity is mediated primarily by a high concentration of positively charged lysines and arginines positioned every third residue within each S4 helix (7). Upon membrane depolarization the S4 helices move through the electric field, activating the channel, which leads to opening of the sodium conduction pathway (8,9).

After activation, the intracellular DIII-DIV linker, acting as a hinged lid, occludes the cytoplasmic side of the channel pore and blocks further ion permeation (10). This process is called "fast inactivation" because it occurs in the millisecond timeframe. Fluorescence recordings revealed that the movement of the S4 helices of DI–DIII occurs on a timescale that corresponds with the activation time constant (11). The S4DIV helix displays a slower component of fluorescence that more closely resembles the time constants of Na_V channel fast inactivation (11). Extracellular immobilization of S4DIV attenuates fast inactivation (12) and mutations of the four most extracellular arginine residues within S4DIV modulate fast inactivation, whereas mutations in S4 helices of other domains typically modulate activation (13–15). Therefore the S4DIV helix is often termed the voltage sensor for fast inactivation.

During depolarization, the voltage sensors in DIII and DIV become immobilized (15–17). Gating currents therefore display biexponential decay upon membrane repolarization. The integral of the fast and slow components of gating current decay represent nonimmobilized and immobilized charge, respectively; up to 60% of the gating charge is immobilized during a 44-ms pulse in $Na_V1.5$ (17). Charge immobilization also occurs with a time course that is similar to fast inactivation (11,15,16). Additionally, disrupting the fast-inactivated state, either through mutations within the S4DIV or by chemically interfering with the inactivation lid, attenuates charge immobilization (13,17). For example, exposing the intracellular membrane to pronase removes both fast inactivation and charge immobilization (8,9).

Extracellular protons destabilize the fast-inactivated state of $Na_V1.5$. Protons slow open-state onset of and accelerate recovery from fast inactivation leading to increased persistent and window currents (19). The majority of effects on fast inactivation by protons occur from the open state (19). Interestingly, charge immobilization occurs faster and with greater magnitude when Na_V channels inactivate from the open state (20,21). We therefore hypothesized that destabilized fast-inactivation during acidosis is the result of protons modulating the kinetics and magnitude of charge immobilization. To test this idea, we expressed $Na_V1.5$ in *Xenopus* oocytes and recorded gating currents using a cut-open voltage-clamp with extracellular solution titrated to either pH 7.4 (control) or pH 6.0. Reducing extracellular pH triggered depolarizing shifts in the Q_{ON}/V and Q_{OFF}/V curves and led to a reduction in the total charge immobilized during depolarization. These data are, to our knowledge, the first reported $Na_V1.5$ gating currents recorded at reduced pH and suggest a molecular basis for the destabilized fast-inactivated state observed in ionic currents during acidosis. These data were previously presented in abstract form (22).

Submitted March 15, 2013, and accepted for publication April 12, 2013.

*Correspondence: pruben@sfu.ca

Editor: Ian Forster.

0006-3495/13/07/0101/7 $2.00

http://dx.doi.org/10.1016/j.bpj.2013.04.022

MATERIALS AND METHODS

Molecular biology

The human variant of the pore-forming α-subunit, hNa$_V$1.5, in SP6-4T was graciously donated by Dr. Chris Ahern (University of British Columbia, Canada). hNa$_V$1.5 DNA was linearized using *Xba*I (Invitrogen, Carlsbad, CA). Transcription was completed using an Sp6 mMESSAGE mMACHINE High Yield Capped RNA Transcription Kit (Applied Biosystems, Carlsbad, CA).

Oocyte preparation

Female *Xenopus laevis* (Boreal Northwest, St. Catharines, Canada) were terminally anesthetized in 2 g/L tricaine solution. Oocytes were surgically removed and theca and follicular layers were enzymatically removed by ~1 h agitation of semiintact lobes in a calcium-free solution containing 96 mM NaCl, 2 mM KCl, 20 mM $MgCl_2$, 5 mM HEPES, and supplemented with 1 mg/mL Type 1A collagenase (Sigma-Aldrich, Oakville, Canada). Oocytes were then washed and sorted in calcium-free solution and finally incubated overnight at 19°C with SOS+ media containing 96 mM NaCl, 2 mM KCl, 1.8 mM $CaCl_2$, 1 mM $MgCl_2$, 5 mM HEPES, 2.5 mM sodium pyruvate, supplemented with 100 mg/L gentamicin sulfate and 5% horse serum. Stage V–VI oocytes were injected with 50 nL of cRNA encoding hNa$_V$1.5. Injected oocytes were incubated at 19°C in SOS+ media for 5–10 days before recording. All surgical and animal care procedures were completed in accordance with the policies and procedures of the Simon Fraser University Animal Care Committee and the Canadian Council of Animal Care (23).

Data acquisition

Macroscopic current recordings were made using a CA-1B amplifier (Dagan, Minneapolis, MN) in the cut-open mode. Data were low-pass-filtered at 10 kHz, digitized at 50 kHz using an ITC-16 interface (HEKA Elektronics, Mahone Bay, Canada), and recorded using Patchmaster version 2x65 (HEKA Elektronics) running on an iMac (Apple Canada, Markham, Canada). Oocytes were placed in a cut-open voltage-clamp triple bath setup, as previously described in Cha et al. (11). Cells were then permeabilized via bottom bath perfusion with intracellular solution containing 120 mM MES, 120 mM NMG, 10 mM HEPES, 2 mM EGTA, titrated to pH 7.4 and supplemented with 0.1% saponin. After 1–2 min exposure, saponin-free intracellular solution was washed in. Extracellular solution of the top and middle chambers contained 120 mM MES, 120 mM NMG, 10 mM HEPES, 2 mM $Ca(MES)_2$. Bath chambers were temperature-controlled at 21°C using a Peltier device run by a TC-10 temperature controller (Dagan, Minneapolis, MN).

Pulse protocols

Cells were maintained at a holding potential of −100 mV between all protocols. Leak subtraction was completed online, using a p/4 protocol from a holding potential of 40 mV. At 40 mV, >99% of voltage sensors are depolarized and therefore small changes in membrane potential do not affect total gating charge. This allowed subtraction of leak current without subtracting the gating current. Because protons reduce tetrodotoxin-Na$_V$1.5 binding affinity (24), ionic currents were blocked using 500 μM tetrodotoxin (TTX) to ensure a saturating concentration of TTX in each recording solution.

Charge-voltage (Q/V) relationships were determined by recording gating currents during 20-ms depolarizations ranging between −130 mV and +60 mV, in 10-mV increments, from a 500-ms, −130 mV prepulse. Measured currents were integrated to determine charge movement, and the charge was plotted as a function of test potential. Charge recovery was measured using a double pulse protocol. The membrane was first depolarized to 0 mV for 500 ms to fully immobilize the gating charge. The membrane was then stepped to a conditioning potential of −120 mV for durations ranging from 0 to 100 ms. The extent of I_{gON} recovery during each conditioning pulse was assessed during a final test pulse to 0 mV. To measure the onset rate of charge immobilization, the membrane potential was held at −130 mV for 100 ms and stepped to a 0-mV conditioning pulse, which varied in duration from 0 to 100 ms. I_{gOFF} was then recorded upon repolarization to −130 mV. All recordings were paired between pH 7.4 and pH 6.0.

Data analysis

Analysis was completed using Fitmaster Ver.. 2x65 (HEKA Elektronics) and Igor Pro v. 5.01 (WaveMetrics, Lake Oswego, OR) run on an iMac (Apple Canada). For Q/V relationships, integrals of I_{gON} and I_{gOFF} were plotted as a function of test potential and fitted with a modified Boltzmann function,

$$f(x) = \frac{(I_1 - I_2)}{\left(1 + \exp\left(-ze_0\left(V_m - V_{1/2}\right)\right)/(kT)\right)} + I_2, \quad (1)$$

where I_1 and I_2 are the maximum and minimum values in the fit, z is the apparent valence, e_0 is the elementary charge, V_m is the membrane potential, $V_{1/2}$ is the midpoint of the curve, T is the recording temperature in °K, and k is the Boltzmann constant. The decay of I_{gOFF} and the integrals of I_{gON} (taken from the recovery protocol and plotted as a function of time) were fitted with a double exponential equation,

$$Y_o + A_1 \exp\left(\frac{-x}{\tau_1}\right) + A_2 \exp\left(\frac{-x}{\tau_2}\right), \quad (2)$$

where Y_0 is the asymptote of the fit, A_1 is the relative component of the first exponent, τ_1 is the slow time constant, A_2 is the relative component of the second exponent, τ_2 is the fast time constant, and x is time. The decay of I_{gON} and the integral of the slow time constant of decay of I_{gOFF} (taken from the onset protocol and plotted as a function of time) were fitted with a single exponential function,

$$f(x) = Y_o + A_1 \exp\left(\frac{-x}{\tau_1}\right), \quad (3)$$

where Y_0 is the asymptote of the fit, A is the relative component of the exponent, τ is the time constant, and x is time.

Statistical analysis was completed using Student's t-test and analysis of variance (ANOVA), where appropriate (INSTAT, GraphPad, La Jolla, CA). All data are reported as mean ± SE and statistical significance was accepted at $p < 0.05$.

RESULTS

Protons depolarize Q/V curves

The β-subunit has limited effects on Na$_V$1.5 activation and fast inactivation in oocytes (2). Moreover, we previously showed that proton modulation of fast inactivation in Na$_V$1.5 is not altered by the β-subunit (19). We therefore assessed proton modulation of Na$_V$1.5 gating currents in the absence of the β-subunit. We recorded Na$_V$1.5 gating currents at different test potentials and calculated the charge-voltage (Q/V) relationship with extracellular

solution titrated to either pH 7.4 or pH 6.0. Gating currents recorded during 20-ms test potentials, from −130 through +60 mV in 10-mV intervals, were integrated, plotted as a function of test potential, and fitted with a Boltzmann function (Eq. 1). Off-gating currents (I_{gOFF}) recorded after a depolarizing pulse were measured before and after the application of 500 μM TTX. Fig. 1, *A–C*, displays sample traces recorded at pH 7.4 as well as pH 7.4 and pH 6.0 in the presence of 500 μM TTX. TTX significantly hyperpolarized the Q_{OFF}/V curve from −37.6 ± 3.01 mV in the absence of TTX to −52.8 ± 4.3 mV in its presence ($n = 6$ and 4, respectively, $p < 0.01$). TTX also significantly reduced the total Q_{OFF} by 16.7 ± 3.1% ($p < 0.01$). Q_{OFF} contamination by ionic tail currents is expected to be negligible in the absence of TTX because fast inactivation typically inhibits >99% of ionic currents, even at reduced extracellular pH (19). These findings are consistent with previous reports that TTX causes hyperpolarizing shifts in Na_V gating (26) and reduces total gating charge (26,27).

In the presence of 500 mM TTX, the $V_{1/2}$ of both the Q_{ON}/V and the Q_{OFF}/V curve were significantly depolarized by extracellular solution titrated to pH 6.0, from −46.2 ± 4.8 mV at pH 7.4 to −36.0 ± 4.4 at pH 6.0 ($n = 6$, $p < 0.05$, Fig. 1 *D*) and −52.8 ± 4.3 mV to −40.3 ± 6.5 mV ($n = 6$, $p < 0.01$, Fig. 1 *E*), respectively. This was expected based on previous work studying the effects of surface charge on channel gating (28). Extracellular pH 6.0 had no effect on the total gating charge or the apparent valence of either the Q_{ON}/V or Q_{OFF}/V curves.

Protons modulate I_g kinetics

Reducing extracellular pH slows open state inactivation, observed as a slowing of the decay of macroscopic ionic current after membrane depolarization (19). A similar effect on the kinetics of $Na_V1.5$ I_{gON} was also observed (Fig. 2, *A* and *C*). We fitted the decay of I_{gON} with a single exponential function (Eq. 3). Previous studies have reported two exponents of decay ($\tau_1 \approx 1$ ms, $\tau_2 \approx 0.1$ ms) (29). The slower τ_1 was dominant at all potentials and τ_2 diminished substantially at more depolarized potentials (>−50 mV) (29). Our signal/noise ratio was insufficient to accurately resolve such a small component of decay; however, our data are comparable to the previously reported dominant component of I_{gON} decay (Fig. 2 *C*) (29). Extracellular pH 6.0 significantly increased the time constant (τ) of decay of I_{gON} at −50 mV and −30 mV through +10 mV, compared to pH 7.4 ($n = 6$, $p < 0.05$, Fig. 2 *C*).

In contrast to the effect on I_{gON}, we observed a trend toward an acceleration of the decay of I_{gOFF} at acidic pH. I_{gOFF} was fitted with a double exponential function and pH 6.0 significantly reduced the τ_{fast} of I_{gOFF} at −40 mV, −30 mV, and +10 mV ($n = 6$, $p < 0.05$, Fig. 2 *B*). Surprisingly, there was no significant change in the time course of the slow component of I_{gOFF} decay (data not shown). pH 6.0

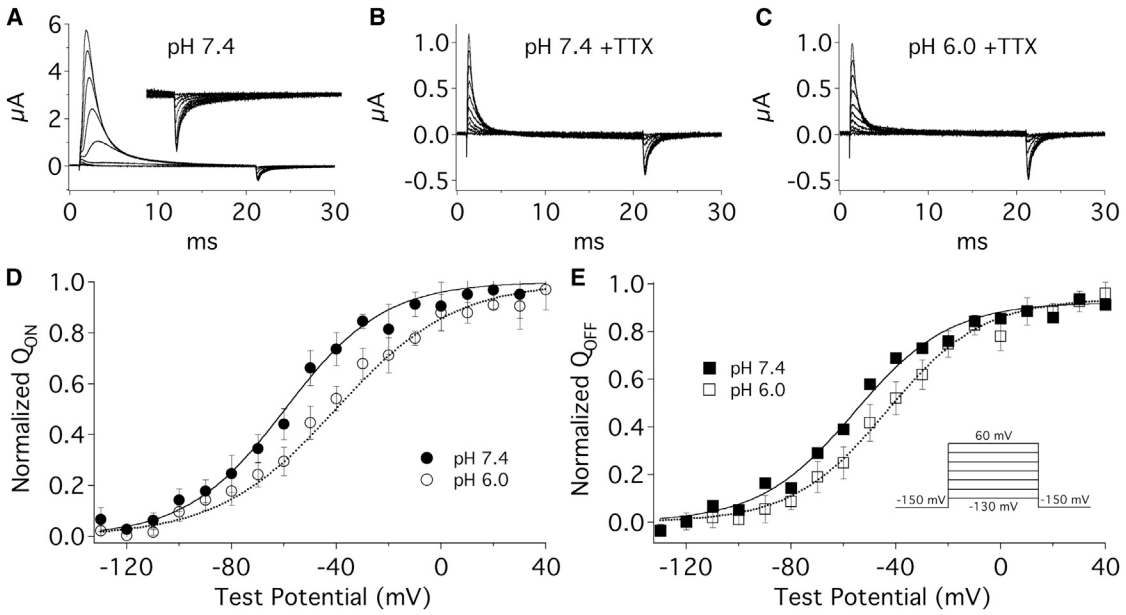

FIGURE 1 Reducing extracellular pH depolarizes the $V_{1/2}$ of $Na_V1.5$ *Q/V* curves. (*A–C*) Sample $Na_V1.5$ gating currents recorded at pH 7.4 (*A*), pH 7.4+TTX (*B*), and pH 6.0+TTX (*C*). (*Inset* in *A*) I_{gOFF} recorded in the absence of TTX but expanded to the same scale as panels *B* and *C*. (*D* and *E*) Normalized charge (*Q*) was plotted as a function of test potential and fitted with a Boltzmann function (Eq. 1). The $V_{1/2}$ of $Na_V1.5$ Q_{ON} (*D*) was significantly depolarized from −46.2 ± 4.8 mV at pH 7.4 (*solid circles*) to −36.0 ± 4.4 mV at pH 6.0 (*open circles*) ($n = 6$, $p < 0.05$). The $V_{1/2}$ of $Na_V1.5$ Q_{OFF} (*E*) was significantly depolarized from −52.8 ± 4.3 mV at pH 7.4 (*solid squares*) to −40.3 ± 6.5 mV at pH 6.0 (*open squares*) ($n = 6$, $p < 0.01$). No significant change was observed in the apparent valence of Q_{ON} or Q_{OFF}. Pulse protocol is displayed in the inset of panel *E*. All data points are mean ± SE.

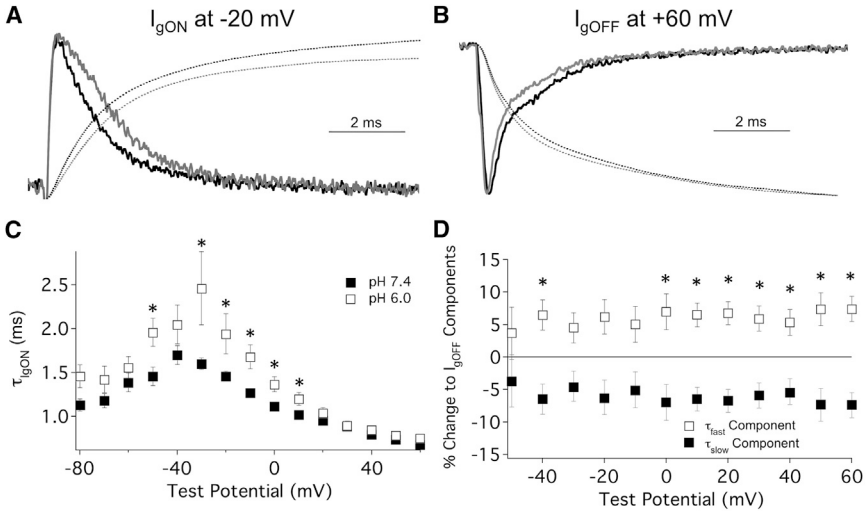

FIGURE 2 Extracellular pH modulates gating current kinetics. (*A* and *B*) Normalized sample I_{gON} traces recorded at −20 mV (*A*) and I_{gOFF} traces recorded at −130 mV after depolarization to +60 mV (*B*) with extracellular solution titrated to pH 7.4 (*solid traces*) and pH 6.0 (*shaded traces*). (*Dotted lines*) Integral of each trace therefore indicates the corresponding Q_{ON} (*A*) and Q_{OFF} (*B*). pH 6.0 significantly accelerated the time course of τ_{fast} of I_{gOFF} at −40 mV, −30 mV, and 10 mV. (*C*) Time constants (τ) of decay from I_{gON} plotted as a function of test potential recorded at pH 7.4 (*solid squares*) and pH 6.0 (*open squares*). pH 6.0 significantly accelerated the τ of I_{gON} at −50 mV and −30 mV through +10 mV. Our data recorded at pH 7.4 are comparable to previous reports of I_{gON} decay recorded under similar conditions (29). (*D*) Change in the relative fast (*open squares*) and slow (*solid squares*) components of I_{gOFF} decay plotted as a function of test potential. pH 6.0 significantly reduced the component of slow decay in I_{gOFF} at −40 mV and 0 mV through +60 mV. The asterisk (*) denotes statistical significance at $p < 0.05$. Pulse protocol from the inset of Fig 1 *E*. $n = 3$–7.

also significantly increased the relative component of the fast decay (and subsequently reduced the relative component of slow decay) in I_{gOFF} at −40 mV and 0 mV through +60 mV ($n = 6$, $p < 0.05$, Fig. 2 *D*). These data demonstrate that reducing extracellular pH slows I_{gON} and accelerates the time course of I_{gOFF}. The slowed I_{gON} and accelerated I_{gOFF} decays, along with the positive shift in the $V_{1/2}$ of each *Q*/*V*, are consistent with a proton-dependent charge screening mechanism. The uniform and voltage-independent shift in the balance of the fast and slow components of I_{gOFF} decay, in conjunction with an unchanged time course of slow I_{gOFF} decay, suggests that there is a reduction in the total charge immobilized after depolarization not attributable to surface charge effects on channel gating (28).

Protons inhibit charge immobilization

Protons destabilize the fast-inactivated state (19). Given the evidence correlating fast inactivation with charge immobilization (8,9,20,21), we hypothesized that charge immobilization is inhibited at acidic extracellular pH. Impaired charge immobilization could underlie the destabilization of the fast-inactivated state at reduced extracellular pH. To test this hypothesis, we directly measured the rates of onset and recovery of charge immobilization at pH 7.4 and pH 6.0.

To assess the rate of charge immobilization onset, Q_{OFF} was recorded 0–110 ms after a 0-mV conditioning pulse. The immobilized charge, calculated from the integral of the slow decay of I_{gOFF}, was normalized to the total Q_{OFF} for that pulse, plotted as a function of time, and fitted with a single exponential function (Eq. 3). The data show that protons significantly increased the time constant for the onset of charge immobilization from 1.1 ± 0.3 ms at pH 7.4 to 1.5 ± 0.4 ms at pH 6.0 ($n = 6$, $p = 0.05$, Fig. 3 *A*). Additionally, we measured the total charge immobilized after a 110-ms pulse to 0 mV. Extracellular protons significantly reduced the maximum probability of charge immobilization from 70.5 ± 5.7% at pH 7.4 to 62.4 ± 6.1% at pH 6.0 ($n = 6$, $p < 0.05$, Fig. 3 *A*).

To assess the recovery of immobilized charge, I_{gON} was integrated 0–100 ms into a −130 mV recovery pulse. Q_{ON} was normalized to the total Q_{ON} and plotted as a function of time. The data were then fitted with a double exponential (Eq. 2, Fig. 3 *B*). Extracellular protons had no effect on the recovery time course of immobilized charge.

DISCUSSION

Previous studies on proton modulation of Na_V channel gating currents, in a variety of tissues, displayed a depolarizing effect on the midpoints of the *Q*/*V* curves but mixed results on the kinetics of I_g decay, total charge, and charge immobilization (30–34). These previous data suggest tissue-specific modulation of gating currents, but did not directly assess proton modulation of a single Na_V channel isoform. Describing $Na_V1.5$ gating current proton modulation contributes to a comprehensive understanding about the effects of protons on $Na_V1.5$ channels and cardiac excitability.

The data presented here, to our knowledge, represent the first $Na_V1.5$ gating current recordings at reduced extracellular pH. We report that lowering the extracellular pH from 7.4 to 6.0 depolarized the $V_{1/2}$ of Q_{ON}/V and Q_{OFF}/V relationships, slowed I_{gON} kinetics, and accelerated fast I_{gOFF} kinetics. These effects are consistent with a charge screening

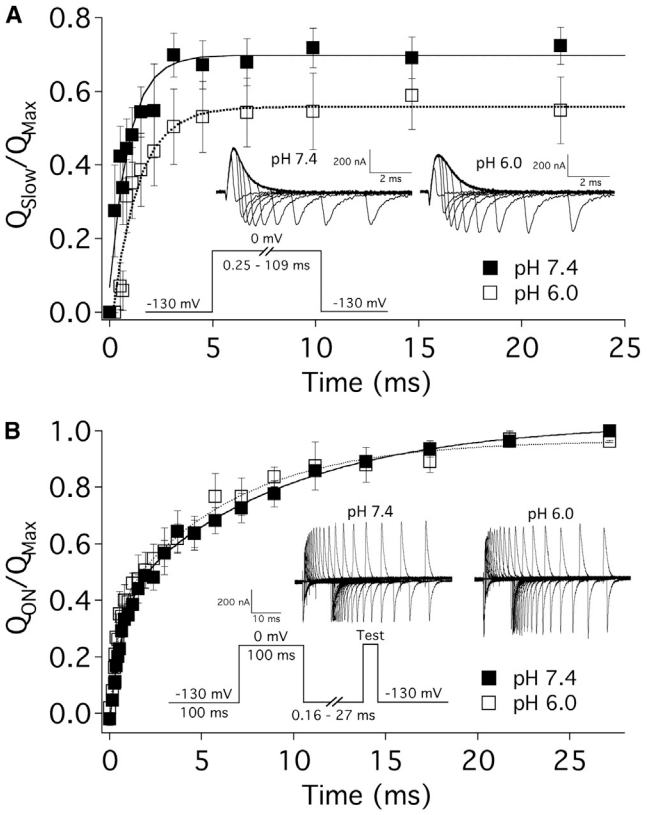

FIGURE 3 Protons slow the onset of gating charge immobilization in $Na_V1.5$. (*A*) To assess the onset of charge immobilization, immobilized charge was normalized to the total Q_{OFF} of each sweep, plotted as a function of time, and fitted with a single exponential function (Eq. 3) for pH 7.4 (*solid squares*) and pH 6.0 (*open squares*). pH 6.0 significantly increased the time constant (τ) of charge immobilization onset from 1.1 ± 0.3 ms to 1.5 ± 0.4 ms and reduced the total charge immobilized from 70.5 ± 5.7 to 62.4 ± 6.1% ($n = 6$, $p < 0.05$). (*Insets*) Pulse protocols used. (*B*) Normalized Q_{ON} is plotted as a function of time and fitted with a double exponential function (Eq. 2). We observed no statistically significant effect on the recovery of gating charge at pH 6.0 (*open squares*) compared to pH 7.4 (*solid squares*) ($n = 5$).

effect. More notably, we demonstrate that protons induce a voltage-independent reduction of slow Q_{OFF} and suggest the resulting acceleration of I_{gOFF} decay kinetics is attributable to reduced charge immobilization and not merely a shift in $Na_V1.5$ voltage-dependence, as would be expected from a charge screening effect (28). The destabilized charge immobilization reported here implies a direct proton-protein interaction, most likely at the extracellular side of the VSD. Our data do not definitively determine whether disruption of charge immobilization by protons leads to destabilized fast inactivation, or whether destabilized fast inactivation by protons affects charge immobilization.

The voltage-sensing domain: a putative proton-binding site

In $Na_V1.5$, the DIVS4 becomes immobilized after activation but before inactivation; the inactivation lid subsequently binds, blocking Na^+ current, and, finally, the DIIIS4 is immobilized (17). Similar results have been observed in $Na_V1.4$ channels (21). If immobilization precedes open-state fast inactivation in $Na_V1.5$, then it seems reasonable to speculate that disruption of charge immobilization would alter fast inactivation. Horn et al. (12) showed that extracellular immobilization of the $Na_V1.4$ DIVS4 with a photoactivated cross linker drastically slowed fast inactivation and increased peak currents (12). Additionally, the site-3 toxin, anthopleurin-A, reduced total charge displacement during depolarization (15). This presumably occurs by inhibiting movement of the S4DIV helix. Anthopleurin-A displays state-dependent binding, concomitantly accelerating fast inactivation and charge immobilization onset at membrane potentials below the threshold of ionic current (<-30 mV in $Na_V1.4$) but slowing fast inactivation and immobilization onset at potentials above threshold (20). These effects underscore the ability of extracellular factors to concurrently modulate charge immobilization and fast inactivation through the VSD of DIV.

In the crystal structure of Na_VAb, the VSD displays a region of negatively charged and polar residues that are predicted to stabilize positively charged arginines of the S4 voltage sensor in its activated state (35). This cluster lines an aqueous cleft that penetrates from the extracellular surface ~10 Å into the VSD, making said arginines readily accessible to protonation (35). The same region in $Na_V1.5$ correlates with a group of Long-QT-syndrome type III-causing mutations, E1225K, E1231K, and E1295K (36,37). Abriel et al. (36) explored the biophysical consequences of these mutations. They reported depolarized voltage dependencies of activation, fast inactivation, and window currents, slowed open-state fast inactivation onset, and accelerated fast inactivation recovery in E1295K compared to wild-type channels (36). These characteristics are remarkably similar to those observed in wild-type channels at reduced extracellular pH (19). These findings underscore the ability of extracellular positive charge at the Na_V channel DIII and DIV VSD to destabilize the fast-inactivated state.

A similar region is present in K_V channels with similar accessibility to positively charged ions (38–40). Most recently, Hoshi and Armstrong (41) demonstrated in *Shaker* channels that application of external La^{3+} displayed a more dramatic effect on the kinetics of gating currents compared to the application of Ca^{2+} (41). These effects were only observed when the cation was applied at hyperpolarized potentials. At depolarized potentials the negatively charged residues form a salt bridge with the positive charged residues of S4, thereby blocking any potential modification by extracellular cations (42–44). and Hoshi and Armstrong (41) postulated that cations such as Ca^{2+} or La^{3+} modulate K_V channel gating by binding extracellular negatively charged residues E183 and E226 found in S1 and S2.

Another possible explanation for our results is that protons exert charge screening, which could explain the

slowing of I_{gON} kinetics and the depolarizing shifts of the Q/V curves. We think this is an unlikely explanation, however, because immobilized charge was reduced even at extreme voltages, i.e., +60 mV (Fig. 2). Strong depolarization would have been expected to rescue total charge immobilization if screening were the sole trigger of the observed effects. Additionally, mutational analysis of proton binding sites within the pore had no effect on proton modulation of channel fast inactivation, so these sites are unlikely to be responsible for proton-dependent changes in charge immobilization (45–47) Therefore, the effects of protons on charge immobilization most likely occur through protonation of extracellular amino-acid residues of the DIII or DIV voltage sensors, thereby disrupting charge immobilization directly.

CONCLUSION

Cations at the extracellular side of the Na_V channel VSD modulate fast inactivation as well as gating charge (11–13,15,17,21,36,37). The data presented herein demonstrate that the immobilization of gating charge is hindered during acidosis. These low pH-induced effects correlate well with the effects previously described on $Na_V1.5$ channel ionic currents and may explain the observed effects of protons on fast inactivation (19). We postulate that protons disrupt charge immobilization leading to the destabilization of the fast-inactivated state, and speculate that this effect occurs through a direct interaction with extracellular carboxylates of the VSDs of DIII or DIV.

The authors thank Stanislav Sokolov for his helpful comments.

This work was funded by Natural Sciences and Engineering Research Council Discovery Grants to P.C.R. and to T.W.C., and a Canadian Foundation for Innovation Leaders Opportunity Fund to T.W.C. and P.C.R. We note that T.W.C. was also supported by a Heart and Stroke Foundation of Canada New Investigator Award and a Michael Smith Foundation for Health Research Career Scholar Award. D.K.J. was supported by a Vanier Graduate Scholarship from the Canadian Institutes for Health Research.

REFERENCES

1. Gellens, M. E., A. L. George, Jr., …, R. G. Kallen. 1992. Primary structure and functional expression of the human cardiac tetrodotoxin-insensitive voltage-dependent sodium channel. *Proc. Natl. Acad. Sci. USA.* 89:554–558.
2. Makita, N., P. B. Bennett, and A. L. George, Jr. 1996. Molecular determinants of β1 subunit-induced gating modulation in voltage-dependent Na^+ channels. *J. Neurosci.* 16:7117–7127.
3. Meadows, L., J. D. Malhotra, …, D. S. Ragsdale. 2001. The intracellular segment of the sodium channel β1 subunit is required for its efficient association with the channel α-subunit. *J. Neurochem.* 76:1871–1878.
4. Noda, M., T. Ikeda, …, S. Numa. 1986. Expression of functional sodium channels from cloned cDNA. *Nature.* 322:826–828.
5. Noda, M., S. Shimizu, …, S. Numa. 1984. Primary structure of *Electrophorus electricus* sodium channel deduced from cDNA sequence. *Nature.* 312:121–127.
6. Terlau, H., S. H. Heinemann, …, S. Numa. 1991. Mapping the site of block by tetrodotoxin and saxitoxin of sodium channel II. *FEBS Lett.* 293:93–96.
7. Stühmer, W., F. Conti, …, S. Numa. 1989. Structural parts involved in activation and inactivation of the sodium channel. *Nature.* 339:597–603.
8. Armstrong, C. M., and F. Bezanilla. 1977. Inactivation of the sodium channel. II. Gating current experiments. *J. Gen. Physiol.* 70:567–590.
9. Bezanilla, F., and C. M. Armstrong. 1977. Inactivation of the sodium channel. I. Sodium current experiments. *J. Gen. Physiol.* 70:549–566.
10. Patton, D. E., J. W. West, …, A. L. Goldin. 1992. Amino acid residues required for fast Na^+-channel inactivation: charge neutralizations and deletions in the III-IV linker. *Proc. Natl. Acad. Sci. USA.* 89:10905–10909.
11. Cha, A., P. C. Ruben, …, F. Bezanilla. 1999. Voltage sensors in domains III and IV, but not I and II, are immobilized by Na^+ channel fast inactivation. *Neuron.* 22:73–87.
12. Horn, R., S. Ding, and H. J. Gruber. 2000. Immobilizing the moving parts of voltage-gated ion channels. *J. Gen. Physiol.* 116:461–476.
13. Kühn, F. J., and N. G. Greeff. 1999. Movement of voltage sensor S4 in domain 4 is tightly coupled to sodium channel fast inactivation and gating charge immobilization. *J. Gen. Physiol.* 114:167–183.
14. Jones, D. K., and P. C. Ruben. 2008. Biophysical defects in voltage-gated sodium channels associated with long QT and Brugada syndromes. *Channels (Austin).* 2:70–80.
15. Sheets, M. F., J. W. Kyle, …, D. A. Hanck. 1999. The Na channel voltage sensor associated with inactivation is localized to the external charged residues of domain IV, S4. *Biophys. J.* 77:747–757.
16. Sheets, M. F., and D. A. Hanck. 2005. Charge immobilization of the voltage sensor in domain IV is independent of sodium current inactivation. *J. Physiol.* 563:83–93.
17. Sheets, M. F., J. W. Kyle, and D. A. Hanck. 2000. The role of the putative inactivation lid in sodium channel gating current immobilization. *J. Gen. Physiol.* 115:609–620.
18. Reference deleted in proof.
19. Jones, D. K., C. H. Peters, …, P. C. Ruben. 2011. Extracellular proton modulation of the cardiac voltage-gated sodium channel, $Na_V1.5$. *Biophys. J.* 101:2147–2156.
20. Groome, J., F. Lehmann-Horn, and B. Holzherr. 2011. Open- and closed-state fast inactivation in sodium channels: differential effects of a site-3 anemone toxin. *Channels (Austin).* 5:65–78.
21. Groome, J. R., M. C. Dice, …, P. C. Ruben. 2007. Charge immobilization of skeletal muscle Na^+ channels: role of residues in the inactivation linker. *Biophys. J.* 93:1519–1533.
22. Jones, D. K., T. W. Claydon, and P. C. Ruben. 2012. Proton modulation of cardiac voltage-gated sodium channel gating currents. *Biophys. J.* 102:326a.
23. Drummond, G. B. 2009. Reporting ethical matters in the *Journal of Physiology*: standards and advice. *J. Physiol.* 587:713–719.
24. Henderson, R., J. M. Ritchie, and G. R. Strichartz. 1974. Evidence that tetrodotoxin and saxitoxin act at a metal cation binding site in the sodium channels of nerve membrane. *Proc. Natl. Acad. Sci. USA.* 71:3936–3940.
25. Reference deleted in proof.
26. Heggeness, S. T., and J. G. Starkus. 1986. Saxitoxin and tetrodotoxin. Electrostatic effects on sodium channel gating current in crayfish axons. *Biophys. J.* 49:629–643.
27. Capes, D. L., M. Arcisio-Miranda, …, B. Chanda. 2012. Gating transitions in the selectivity filter region of a sodium channel are coupled to the domain IV voltage sensor. *Proc. Natl. Acad. Sci. USA.* 109:2648–2653.
28. Cukierman, S., W. C. Zinkand, …, B. K. Krueger. 1988. Effects of membrane surface charge and calcium on the gating of rat brain sodium channels in planar bilayers. *J. Gen. Physiol.* 92:431–447.

29. Sheets, M. F., and D. A. Hanck. 1995. Voltage-dependent open-state inactivation of cardiac sodium channels: gating current studies with Anthopleurin-A toxin. *J. Gen. Physiol.* 106:617–640.

30. Keynes, R. D., and E. Rojas. 1974. Kinetics and steady-state properties of the charged system controlling sodium conductance in the squid giant axon. *J. Physiol.* 239:393–434.

31. Wanke, E., P. L. Testa, …, E. Carbone. 1983. High intracellular pH reversibly prevents gating-charge immobilization in squid axons. *Biophys. J.* 44:281–284.

32. Schauf, C. L. 1983. Evidence for negative gating charges in *Myxicola* axons. *Biophys. J.* 42:225–231.

33. Neumcke, B., W. Schwarz, and R. Stämpfli. 1980. Increased charge displacement in the membrane of myelinated nerve at reduced extracellular pH. *Biophys. J.* 31:325–331.

34. Campbell, D. T. 1983. Sodium channel gating currents in frog skeletal muscle. *J. Gen. Physiol.* 82:679–701.

35. Payandeh, J., T. Scheuer, …, W. A. Catterall. 2011. The crystal structure of a voltage-gated sodium channel. *Nature.* 475:353–358.

36. Abriel, H., C. Cabo, …, R. S. Kass. 2001. Novel arrhythmogenic mechanism revealed by a long-QT syndrome mutation in the cardiac Na^+ channel. *Circ. Res.* 88:740–745.

37. Tester, D. J., M. L. Will, …, M. J. Ackerman. 2005. Compendium of cardiac channel mutations in 541 consecutive unrelated patients referred for long QT syndrome genetic testing. *Heart Rhythm.* 2:507–517.

38. Starace, D. M., and F. Bezanilla. 2001. Histidine scanning mutagenesis of basic residues of the S4 segment of the *Shaker* K^+ channel. *J. Gen. Physiol.* 117:469–490.

39. Starace, D. M., E. Stefani, and F. Bezanilla. 1997. Voltage-dependent proton transport by the voltage sensor of the *Shaker* K^+ channel. *Neuron.* 19:1319–1327.

40. Starace, D. M., and F. Bezanilla. 2004. A proton pore in a potassium channel voltage sensor reveals a focused electric field. *Nature.* 427:548–553.

41. Hoshi, T., and C. M. Armstrong. 2012. Initial steps in the opening of a *Shaker* potassium channel. *Proc. Natl. Acad. Sci. USA.* 109:12800–12804.

42. Long, S. B., E. B. Campbell, and R. MacKinnon. 2005. Crystal structure of a mammalian voltage-dependent *Shaker* family K^+ channel. *Science.* 309:897–903.

43. Fernandez, D., A. Ghanta, …, M. C. Sanguinetti. 2005. Molecular mapping of a site for Cd^{2+}-induced modification of human ether-à-go-go-related gene (hERG) channel activation. *J. Physiol.* 567:737–755.

44. Abbruzzese, J., F. B. Sachse, …, M. C. Sanguinetti. 2010. Modification of hERG1 channel gating by Cd^{2+}. *J. Gen. Physiol.* 136:203–224.

45. Jones, D. K., C. H. Peters, …, P. C. Ruben. 2013. Proton sensors in the pore domain of the cardiac voltage-gated sodium channel. *J. Biol. Chem.* 288:4782–4791.

46. Khan, A., J. W. Kyle, …, H. A. Fozzard. 2006. Isoform-dependent interaction of voltage-gated sodium channels with protons. *J. Physiol.* 576:493–501.

47. Khan, A., L. Romantseva, …, H. A. Fozzard. 2002. Role of outer ring carboxylates of the rat skeletal muscle sodium channel pore in proton block. *J. Physiol.* 543:71–84.